Journal of Materials Chemistry C

ROYAL SOCIETY OF CHEMISTRY

COMMUNICATION

View Article Online
View Journal | View Issue

Cite this: *J. Mater. Chem. C*, 2022, **10**, 9938

Received 18th May 2022,
Accepted 8th June 2022

DOI: 10.1039/d2tc02055f

rsc.li/materials-c

"Green" synthesis of highly luminescent lead-free $Cs_2Ag_xNa_{1-x}Bi_yIn_{1-y}Cl_6$ perovskites†

Oleksandr Stroyuk,*[a] Oleksandra Raievska,[a] Anastasia Barabash,[b] Miroslaw Batentschuk,[b] Andres Osvet,[b] Saskia Fiedler,[c] Ute Resch-Genger,[c] Jens Hauch[ab] and Christoph J. Brabec[ab]

A new "green" and mild synthesis of highly stable microcrystalline $Cs_2Ag_xNa_{1-x}Bi_yIn_{1-y}Cl_6$ (CANBIC) perovskites under ambient conditions was developed that is scalable to the multi-gram production. Under UV illumination, the CANBIC perovskites emit intense broadband photoluminescence (PL) with a quantum yield (QY) of 92% observed for x = 0.35 and y = 0.01–0.02. The combination of strong UV absorbance and broadband visible emission, high PL QY, and long PL lifetimes of up to 1.4 μs, along with an outstanding stability makes these CANBICs a promising material class for many optical applications.

Lead halide perovskites have gone through an unprecedented rapid development from one of many promising photovoltaic materials to a real competitor for established photovoltaic absorbers such as silicon, copper–indium–gallium chalcogenides, and CdTe.[1–4] This triggered the search for novel lead-based perovskite compounds and particularly for "greener" lead-free structural analogs with comparable optical and photovoltaic characteristics. Due to the many possible compositions of lead-free perovskites (LFPs), especially of the so-called double LFPs with a couple of Pb^{2+} being substituted by M^+M^{3+} combinations,[1,3] there are hundreds of structures which could be identified as promising candidates for photovoltaics, light emission, and light management (down-shifting, up-conversion, *etc.*).[1,3–6] Given the broad variability of alkali metal and halide positions in LFPs, these structures translate into thousands of compounds to be synthesized and tested for light-conversion applications which presents a huge experimental challenge.

LFP tunability can be exemplified by In-based double compounds, $A_2M^{I}InX_6$ (A – alkali metals, X – halides), where all four positions can be independently varied. In particular, M^{I} can be occupied by Na^+, K^+, Ag^+ or their mixtures, A – by Cs^+, Rb^+, or organic cations, and X – by individual and mixed halides. At the same time, In^{III} can be substituted by a number of M^{III} cations, including Bi^{III} and Sb^{III}.[1,4] The interest in such compounds, particularly in Bi-doped $Cs_2Ag_xNa_{1-x}InCl_6$ (referred to as CANIC) or $Cs_2Ag_xNa_{1-x}Bi_yIn_{1-y}Cl_6$ (referred to as CANBIC), is constantly growing due to their intense broadband photoluminescence (PL) combined with a unique tunability of the photophysical properties and an outstanding chemical stability.[5–21]

In view of this compositional variability, the progress in the material science of LFP requires a transition from conventional single-compound trials to high-throughput studies based on robot-assisted synthesis and characterization, ideally supported by machine-learning-based data analysis.[22–24] The feasibility and efficiency of high-throughput experiments in the field of lead perovskite photovoltaics were recently demonstrated.[25–30]

However, the majority of the reported syntheses of double LFPs require high energy input by hydrothermal treatment or calcination. Furthermore, a considerable amount of manual intermediate steps is needed which cannot be automated, as well as the usage of hazardous chemicals such as concentrated HCl in the case of chloride LFPs[1,3,6,7,9,14,17,21] or unstable and aggressive substances for bromide and iodide LFPs.[1,3,21] More favorable milder temperature-, saturation-, or antisolvent-driven precipitation approaches, conventionally employed for the fabrication of lead-based perovskites, often yield poorly controlled mixtures of perovskite and non-perovskite phases when applied to double LFPs.[1,13,31] As a result, the development of simple and mild procedures for the reproducible and phase-controlled synthesis of double LFPs under ambient conditions with robotized equipment still remains challenging.

In this communication, we introduce such an approach to the fabrication of microcrystalline lead-free CANIC and CANBIC perovskites, yielding compositionally controlled single-phase products under ambient conditions in a single step without any

[a] *Forschungszentrum Jülich GmbH, Helmholtz Institute Erlangen-Nuremberg for Renewable Energies (HI ERN), 91058 Erlangen, Germany*
E-mail: o.stroyuk@fz-juelich.de
[b] *Friedrich-Alexander Universität Erlangen-Nürnberg, Materials for Electronics and Energy Technology (i-MEET), Martensstrasse 7, 91058, Erlangen, Germany*
[c] *Federal Institute for Materials Research and Testing (BAM), Division Biophotonics, 12489 Berlin, Germany*

† Electronic supplementary information (ESI) available. See DOI: https://doi.org/10.1039/d2tc02055f

additional thermally activated steps or the need for hazardous chemicals. By focusing on the optical properties of the most strongly emissive CANBIC perovskite composition, we show that our approach results in a very stable and structurally perfect material emitting broadband PL in the visible spectral range with a PL quantum yield (QY) close to unity.

Synthesis and characterization of CANBIC perovskites

Synthesis

$Cs_2Ag_xNa_{1-x}InCl_6$ (CANIC) and $Cs_2Ag_xNa_{1-x}Bi_yIn_{1-y}Cl_6$ (CANBIC) perovskites were synthesized at room temperature under ambient atmosphere *via* the combination of two precursor solutions in 2-propanol:water mixtures, one of them containing a minimal amount of HCl to prevent hydrolytic reactions of Bi^{3+} and In^{3+} ions. A stock $InCl_3$ solution (1.0 M) was first prepared in 1.0 M HCl. In a similar manner, a stock $BiCl_3$ solution (1.0 M) in 4.0 M HCl was made. Stock solutions of silver(I) nitrate (1.0 M), sodium acetate (4.0 M) and cesium acetate (4.0 M) were prepared in deionized (DI) water.

Two stable and transparent precursor solutions were prepared for the synthesis of the perovskites as described below. Precursor solution I was then mixed with precursor solution II under vigorous stirring and the resulting sample was kept at ambient conditions for 60 min to allow crystallization. The most luminescent CANBIC sample with $x = 0.35$ and $y = 0.02$ was chosen to be described in more detail below. Precursor solution I was prepared by adding 2 μL stock 1.0 M $BiCl_3$ solution (in 4.0 M HCl), 98 μL 1.0 M stock $InCl_3$ solution (in 1.0 M HCl), 0.10 mL concentrated 37 w% (12 M) HCl, and 0.5 mL 2-propanol to an Eppendorf vial. The acid can be mixed with 2-propanol beforehand to avoid HCl evaporation and used as a single reactant. Precursor solution II was prepared by mixing 0.5 mL 2-propanol with 0.1 mL DI water, 0.04 mL aqueous 1.0 M $AgNO_3$ solution, and 0.025 mL aqueous 5.0 M ammonia solution in an Eppendorf vial under continuous stirring. Ammonia was added to form an Ag(I)–NH_3 complex to avoid the formation of silver hydroxide upon interaction with alkaline solutions of Cs(I) and Na(I) acetates. Subsequently, 0.025 mL 4.0 M aqueous NaAc (Ac = acetate) and 0.06 mL aqueous 4.0 M CsAc solutions were added at intense stirring. The as-precipitated perovskite was separated from the supernatant, 1 mL of pure 2-propanol added, and the mixture centrifuged at 5000 rpm for 3 min. The precipitate was separated, and the procedure of 2-propanol addition and centrifugation was repeated.

Characterization

The structural parameters and the chemical composition of the samples (powders and samples deposited on substrates) were characterized by X-ray diffraction (XRD), scanning electron microscopy (SEM), and cathodoluminescence (CL) imaging. Details of the characterization techniques are provided in the ESI.† The perovskite samples were also characterized with reflectance, PL, and Raman spectroscopy, as well as time-resolved PL spectroscopy, and X-ray photoelectron spectroscopy (XPS). The PL QY of the perovskite samples was absolutely determined using a calibrated Quantaurus spectrometer (Hamamatsu) with ultrapure $BaSO_4$ powder (Thermo Fisher) as a blank.

General description of the synthetic protocol

We developed a simple and "green" approach for the synthesis of CANIC and CANBIC perovskites which can be performed under ambient conditions without annealing, boiling, or hydrothermal treatment. The formation of perovskites occurs upon the contact of two stable and transparent precursor solutions, thereby avoiding the formation of secondary phases and achieving elemental and structural homogeneity. For this process, an excess of sodium with respect to the stoichiometric amount is necessary to drive the precipitation towards the formation of perovskite CAN(B)IC phases instead of forming less soluble Ag–M–Cl phases. Therefore, the Na-to-Ag content was varied by introducing different amounts of silver nitrate in the presence of a constant excess of sodium acetate (NaAc).

The addition of a 20% excess of Cs^+ results in more luminescent and stable CAN(B)IC perovskites. This is ascribed to the suppression of the formation of non-luminescent ternary Cs–M–Cl phases, for example, $Cs_3M_2Cl_9$ (with Cs : M = 1.5 : 1) instead of CAN(B)IC compounds, where the Cs : M ratio equals to 2 : 1. Excessive Na^+ and Cs^+ are removed during the purification stage. Fig. 1a schematically summarizes the composition of both precursor solutions and the synthetic procedure which is followed by an optimization of the composition of CANBIC perovskites to reach a maximum PL efficiency. The latter is illustrated by photographs taken under ambient and UV illumination shown in Fig. 1b and c.

To identify CANBICs with optimum performance, a compositional screening was performed, using PL QY as the key performance parameter. Therefore, we varied the ratios of the metal components of the CANBIC perovskites and the reaction temperature.

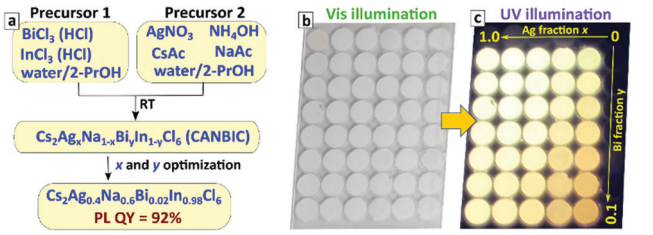

Fig. 1 (a) Schematic of the CANBIC perovskite synthesis. (b and c) Photographs of a set of CANBIC samples with varied x and y taken under (b) ambient light and (c) UV illumination at 370–390 nm.

Ag-to-Na ratio

As previously reported, CANBIC perovskites show a strong dependence of their PL QY on the Ag-to-Na ratio with a maximum PL QY, often found for $x = 0.4$.[5,6,19] To find the best Ag-to-Na ratio, we assessed the PL behavior of a series of perovskites with a constant Bi content ($y = 0.02$), while varying the nominal silver fraction calculated as $r_{Ag} = [Ag^+]/([Ag^+] + [Na^+])$. Here, the integral PL intensity and PL lifetime (see a more detailed discussion below) were used as key performance parameters as shown in Fig. 1b and c. The maximum PL intensity was found for r_{Ag} close to 0.30 (Fig. S1, ESI†). A similar trend was observed for the PL lifetime with a maximum of *ca.* 1.4 μs at $r_{Ag} = 0.30$. Subsequently performed EDX measurements of this particular sample confirmed a molar Ag fraction of $x = 0.35$.

Cs content

Our synthetic procedures rely on the ionic equilibria in the precursor and the final reaction mixtures. Therefore, the presence of excess amounts of Na^+ and Cs^+ is required for the complete crystallization of the CANBIC perovskites and high PL efficiencies. We examined the effect of the nominal Cs-to-In molar ratio chosen for the synthesis on the PL intensity and PL dynamics (Fig. S2, ESI†). The maximum of both PL intensity and PL lifetime was found for a Cs-to-In molar ratio of 2–3.

Temperature

Subsequently, the effect of the reaction temperature, varied from 10 °C to 90 °C, on the PL properties of the resulting perovskites was studied. The highest PL intensity and the longest PL lifetime were found for a reaction temperature as low as 22 °C (Fig. S3, ESI†). Raman spectroscopic studies of CANBIC powders produced at varied Ag-to-Na ratios, varying Cs content, and different temperatures confirm that all samples have an identical perovskite structure, except for two samples where neither Ag nor Cs were introduced to the precursors (Fig. S4, ESI†).

Bi-to-In ratio

As a platform for Bi-doping, we used CANBIC perovskites with optimized Ag and Cs content synthesized at an optimum reaction temperature where the Bi content was varied from $y = 0.002$ to 0.05. EDX measurements shown in the next section confirmed the good match between the nominal and real y values within the entire range of studied Bi-to-In ratios. PL studies revealed the dependence of the PL intensity on the parameter y (Fig. S5a, ESI†) with a maximum observed for 1–2 mol% Bi, smaller and larger Bi contents showing lower PL intensities. At the same time, both the bandgap and the PL lifetime decreased almost linearly with increasing Bi content in the entire probed range (Fig. S5b and c, ESI†). Therefore, the most luminescent CANBIC sample with 2 mol% of Bi doping was selected for further in-depth characterization and PL studies. The brutto-formula of the selected sample derived from the EDX data is $Cs_2Ag_{0.35}Na_{0.65}Bi_{0.02}In_{0.98}Cl_6$.

Structural characterization of CAN(B)IC

SEM imaging of the CANIC perovskite revealed its polygonal crystal structure with individual sizes of 1–5 μm (Fig. S6, left image, ESI†). Introduction of 2% Bi(III) resulted in a shift of crystal size distribution to *ca.* 0.5–3 μm (Fig. S6, right image, ESI†), indicating a restrictive effect of Bi(III) doping on the crystal growth.

Another remarkable feature of CANBIC crystals is a very strong cathodoluminescence (CL), while CANIC crystals did not show CL at all. The SEM images of the CANBIC sample registered using secondary electron contract and CL contrast are shown in Fig. 2a and b, respectively. Both images are identical indicating a uniform distribution of emission centers in the CANBIC crystals.

EDX analysis of the CANBIC sample performed at three different positions within the samples (Fig. 2c) revealed an identical elemental distribution for all three points, confirming the excellent compositional homogeneity of the sample. The real y values determined from the measured elemental ratios were always close to the nominal ones used for perovskite synthesis). As shown in Table 1, the ratios of Cs and Cl to the sum of In + Bi are close to 2 and 6, respectively, as expected from the nominal compositions. X-ray photoelectron (XPS) spectra of CANIC and CANBIC (Fig. S7, ESI†) confirmed the presence of silver, indium, and, in the case of CANBIC, also bismuth cations in the expected oxidation states: Ag(I), In(III), and Bi(III).[32]

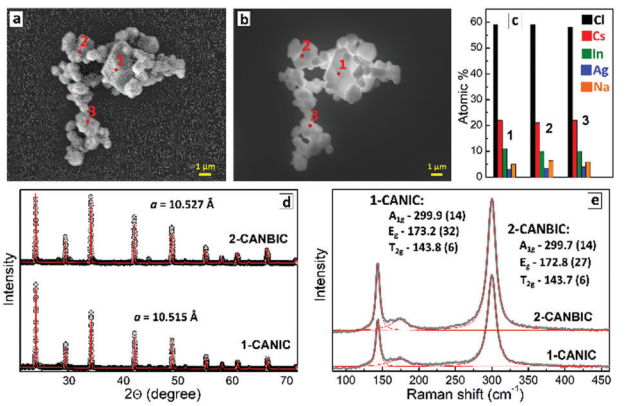

Fig. 2 (a and b) SEM images of CANBIC microcrystals registered using secondary electron contrast (a) and CL contrast (b). (c) Elemental composition of CANBIC crystals determined by EDX at three points indicated in (a and b). (d) X-ray diffractograms of CANBIC (top) and CANIC (bottom) perovskites. The gray circles correspond to experimental data, red solid lines – to data derived from a Rietveld refinement analysis. (e) Raman spectra of CANIC (curve 1) and CANBIC (curve 2) perovskites, where gray lines represent the experimentally obtained spectra, and the red lines show Lorentzian fits. Abbreviations: CANIC – $Cs_2Ag_{0.35}Na_{0.65}InCl_6$, CANBIC – $Cs_2Ag_{0.35}Na_{0.65}Bi_{0.02}In_{0.98}Cl_6$.

Table 1 Elemental composition of CANIC and CANBIC perovskites determined by EDX

	Nominal x	Nominal y	Real x	Real y	Cs-to-M ratio	Cl-to-M ratio
CANIC	0.4	0	0.35 ± 0.10	0	2.1 ± 0.1	5.8 ± 0.3
CANBIC	0.4	0.02	0.35 ± 0.10	0.02 ± 0.01	2.1 ± 0.1	6.2 ± 0.3

The XRD pattern of the undoped CANIC perovskites presented in Fig. 2d (bottom) exhibit the typical reflections for cubic perovskites with the lattice of *Fm3m* space group.[7–9,11,12,14,17,21] The lattice parameter derived *via* a Rietveld refinement procedure, a = 10.515 Å, is close to the reported values. As can been seen in the top panel of Fig. 2d, the introduction of 2 mol% Bi did not change the structure of the XRD pattern, indicating that Bi(III) substitutes In(III) without affecting the lattice type. However, a small lattice expansion (a = 10.527 Å) was observed due to the larger ionic radius of Bi(III) as compared to In(III).[6–8,12]

The Raman spectrum of CANIC perovskite, shown in Fig. 2e (curve 1), reveals three major vibrations at approximately 300 cm^{-1}, 173 cm^{-1}, and 144 cm^{-1} which can be assigned to A_{1g}, E_g, and T_{2g} modes of the CANIC lattice, respectively.[8,9,14,17] Thereby, also Raman spectroscopy confirmed that the introduction of 2% Bi(III) led only to minor peak shifts (Fig. 2e, curve 2) due to the In-to-Bi exchange but no structural changes. Both XRD and Raman results suggest that Bi-doping is not accompanied by the formation of additional phases or changes in the perovskite structure. Despite the high PL intensity of CANBIC under UV excitation, Raman spectra can be reliably measured without a noticeable PL background using a non-resonant excitation at 532 nm. The fact indicates a high quality of the CANBIC lattice, with a very low population of the mid-bandgap states related to lattice defects.

Spectroscopic properties of CAN(B)IC perovskites

Absorption and PL

Doping with 2% Bi resulted in a "red" shift of the optical bandgap, from about 3.5–3.6 eV (345–355 nm) for CANIC (Fig. 3a, curve 1) to *ca.* 3.0 eV (410 nm) for CANBIC (Fig. 3a, curve 2), as well as the formation of a distinct absorption peak at approx. 3.3 eV (375 nm).

CANBIC perovskites showed a broad PL band from 450–900 nm centered at about 590–595 nm or *ca.* 2.1 eV (Fig. 3a, curve 3). The large Stokes shift as well as the large spectral width of the PL band indicate that the PL is emitted *via* the self-trapped exciton (STE) mechanism which is typical for doped/alloyed lead-free halide perovskites.[6,19,33] The PL excitation (PLE) spectrum recorded in the center of the PL band (Fig. 3a, curve 4) perfectly matches with the absorption spectrum suggesting that the PL emission solely originates from light absorption in the fundamental band. In contrast, CANIC perovskite showed only a negligible emission.

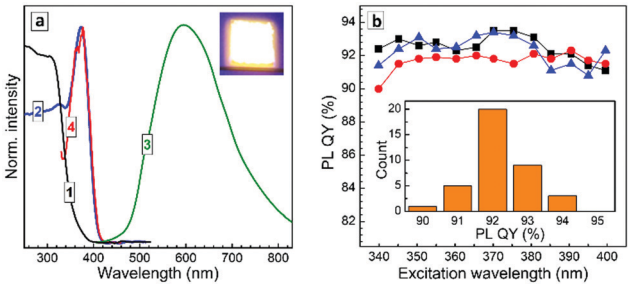

Fig. 3 (a) Normalized absorption (1, 2), PL emission (3), and PL excitation (4) spectra of CANIC (curve 1) and CANBIC (curves 2–4) perovskites. (b) PL QY of three CANBIC samples (series denoted by circles, rectangles and triangles) measured at different excitation wavelengths. Inset: Distribution of PL QY values measured at different excitation wavelengths.

The drastic enhancement of both absorption and PL emission is typically related to a decisive influence of the dopant on the lattice symmetry of the perovskite matrix, even at very low dopant contents.[4,6,9,17] The introduction of Bi(III) breaks the symmetry of the perovskite lattice and converts the interband transitions from symmetry-forbidden to allowed ones, thereby greatly increasing the oscillator strength as compared to pristine CANIC.[4,6,9,12,14,17,20,33] The emission color of our CANBIC sample(s) is a warm white-yellow (inset in Fig. 3a) with the CIE color coordinates of X = 0.43, Y = 0.50, and a color temperature of about 3700 K (Fig. S8a, ESI†).

PL QY measurements

The PL QY was absolutely measured at room temperature for three separately prepared batches of CANBIC of the same composition, and recorded at different excitation wavelengths ranging from 340 nm to 400 nm. These measurements revealed a very high PL with an average PL QY (averaged for all three samples and all excitation wavelengths) of 92% and a statistical uncertainty of ±2% (Fig. 3b). This value is the highest reported so far for microcrystalline CANBIC perovskites; comparable PL QY were obtained by Sargent *et al.* for 0.04% Bi doping (86%)[6] and by Wang *et al.* for 1% Bi doping (*ca.* 90%).[34] More examples of reports on highly-luminescent double In/Bi-based perovskites are presented in Table S1 (ESI†).

The PL QY uncertainty reported here (2%) reflects the relative standard deviation observed in our experiments rather than the inherent uncertainty of such measurements including instrument calibrations, which is approximately 5%.[35,36]

Stability tests

The CANBIC perovskite samples were very stable when stored under ambient conditions. No changes in PL properties (PL intensity, peak position and spectral width) were detected after five months of storage at room temperature, ambient humidity, and diffuse illumination (Fig. S9a, ESI†). Heating to 200 °C for 30 min did not change the spectral position of the PL bands, while a decrease of PL intensity was observed at 300 °C (Fig. S9b, ESI†). The samples heated to 400 °C showed both a coloration (yellow-brown) and a strong PL quenching. However,

a prolonged (up to 6 h) treatment of the CANBIC perovskite at 150 °C (below the thermal damage threshold) caused no appreciable changes in the PL intensity (Fig. S9c, ESI†).

The CANBIC sample showed also no changes in the PL intensity when subjected to UV illumination for 12 h under ambient atmosphere attesting to a high photochemical stability.

Time-resolved PL

Time-resolved PL studies revealed complex decay kinetics, with deviation from a single-exponential decay (Fig. 4a) depending on the perovskite composition. To simultaneously extract the PL lifetime and to evaluate the deviation from single-exponential decay kinetics, we fitted the curves with a stretched-exponential function $I(t) = I_0 \exp\left(\left(-\frac{t}{\tau}\right)^{1/h}\right)$.[5,20,37,38] These fits provide a characteristic PL time τ and a heterogeneity parameter h, which is equal to unity for single-exponential decay and larger than 1 for more complex decay kinetics. For solid samples, the heterogeneity parameter is often regarded as a measure for random fluctuations of the lattice or local defects close to the radiative recombination sites resulting in a variation of the emission lifetime even for a single emitting state.[37–39]

We focused here on the PL dynamics of the CANBIC perovskites prepared with a varied Ag-to-Na ratio at room temperature (Fig. 4). Two sets of samples were studied, the first one systematically varying the Ag content at a constant Na content (squares in Fig. 4b), and the second one varying the Na(I) content at a constant Ag content (circles in Fig. 4b). Thereby, the entire range of r_{Ag} = 0.1 could be covered.

No PL was detected for compounds containing only Na(I), as discussed above. As the nominal r_{Ag} in the precursor solution was elevated, the PL lifetime was considerably increased and revealed the same trend as the PL efficiency, reaching a maximum value of about 1.4 μs at r_{Ag} = 0.30 (Fig. 4b, scatters 1), corresponding to x = 0.35 (see EDX analysis). At higher Ag(I) content, the average PL lifetime gradually decreased to approximately 0.5 μs for x = 1.00. The heterogeneity factor showed an opposite trend, reaching a minimum value of about 1.1 at r_{Ag} = 0.30–0.40 (Fig. 4b, scatters 2), that is, in the range of the highest PL efficiencies observed. For these compositions, the PL decay curves showed almost single-exponential behavior, indicating a high degree of lattice perfection and a narrow distribution of possible STE energies.

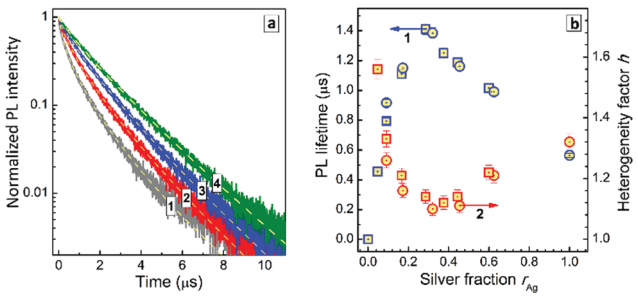

Fig. 4 (a) PL decay curves of CANBIC perovskites with a nominal ratio r_{Ag} = [Ag$^+$]/([Ag$^+$] + [Na$^+$]) of 0.05 (curve 1), 0.10 (2), 0.15 (3), and 0.30 (4) recorded at room temperature using an excitation wavelength of 402 nm. The dashed lines represent fits of the PL decay curves with a stretched exponential function. (b) Average PL lifetime (blue squares/circles, set 1) and heterogeneity factor h (red squares/circles, set 2) calculated for CANBIC perovskites produced with varied r_{Ag}. The squares represent a CANBIC series with varied [Ag$^+$] at constant [Na$^+$] and the circles a series with a varied [Na$^+$] at constant [Ag$^+$].

In conclusion, we introduced a new mild and "green" approach for the synthesis of lead-free microcrystalline $Cs_2Ag_xNa_{1-x}Bi_yIn_{1-y}Cl_6$ (CANBIC) perovskites, which does not require volatile solvents or concentrated acids, and can be performed at room temperature. The CANBIC composition was optimized with respect to the photoluminescence (PL) intensity, with the highest PL observed for $Cs_2Ag_{0.35}Na_{0.65}Bi_{0.02}In_{0.98}Cl_6$. This optimized CANBIC perovskite emitted a broadband PL centered at *ca.* 2.1 eV (590–595 nm) with a PL quantum yield of 92% at room temperature. This value is among the highest ones reported so far for this class of lead-free perovskite compounds. The PL dynamics depended strongly on the perovskite composition, with the most luminescent CANBIC (x = 0.35, y = 0.02) revealing an almost single-exponential PL decay with an average PL lifetime of about 1.4 μs at room temperature. Moreover, the emissive characteristics of CANBIC are stable at prolonged shelf-storage, moderate heating, and under UV illumination. This underlines the huge potential of CANBIC perovskites for a variety of applications as optical and electro-optical components in devices and down-converters. As a particular practical example, the application of CANBIC in luminescent solar light concentrators for silicon photovoltaics can be envisaged, favoured by a negligible overlap between the absorption and emission spectra of the perovskite as well as by a perfect match between the PL spectrum of CANBIC and the absorption spectrum of Si. Additionally, the CANBIC perovskite exhibited bright cathodoluminescence making this material promising for the detection of high-energy irradiation and applications as a scintillating material.

Overall, our new "green" synthesis procedure for CANBIC perovskites with varying composition showed an excellent reproducibility and can be easily scaled up to multi-gram amounts. Also, it presents a promising route for future high-throughput experiments aiming for a more detailed investigation of the structure property relationships in the large compositional space of CANBIC perovskites.

Author contributions

O. Stroyuk: conceptualization (lead), investigation (equal), writing – original draft preparation (lead); O. Raievska: investigation (lead), methodology (lead); A. Barabash – investigation (equal); M. Batentschuk – resources (equal), writing – review & editing (equal); A. Osvet – investigation (equal), resources (equal); S. Fiedler: investigation (equal), writing – review & editing (equal); Ute Resch-Genger: resources (equal), writing – review & editing (equal), J. Hauch: conceptualization (equal),

project administration (lead), writing – review & editing (equal); C. Brabec: conceptualization (equal), funding acquisition (lead), writing – review & editing (equal).

Conflicts of interest

The authors declare no conflicts of interests.

Acknowledgements

The authors gratefully acknowledge financial support of The German Federal Ministry for Economic Affairs and Climate Action (OS, OR, JH, and CB: project Pero4PV, FKZ 03EE1092A; UR and SF: program WIPANO, project MeLuQuanPhosphor) and The Bavarian State Government (project ''ELF-PV-Design and development of solution processed functional materials for the next generations of PV technologies'', no. 44-6521a/20/4). UR and SF gratefully acknowledge support with the measurements and data evaluation by Dipl.-Ing. Arne Güttler and Dr Christian Würth.

Notes and references

1 H. Tang, Y. Xu, X. Hu, Q. Hu, T. Chen, W. Jiang, L. Wang and W. Jiang, *Adv. Sci.*, 2021, **8**, 2004118.
2 A. Dey, J. Ye, A. De, E. Debroye, S. K. Ha, E. Bladt, A. S. Kshirsagar, Z. Wang, J. Yin and Y. Wang, *et al.*, *ACS Nano*, 2021, **15**, 10775.
3 N. K. Tailor, S. Kar, P. Mishra, A. These, C. Kupfer, H. Hu, M. Awais, M. Saidaminov, M. I. Dar, C. Brabec and S. Satapathi, *ACS Mater. Lett.*, 2021, **3**, 1025.
4 S. Li, J. Luo, J. Liu and J. Tang, *J. Phys. Chem. Lett.*, 2019, **10**, 1999.
5 L. Zdražil, S. Kalytchuk, M. Langer, R. Ahmad, J. Pospíšil, O. Zmeškal, M. Altomare, A. Osvet, R. Zbořil, P. Schmuki, C. J. Brabec, M. Otyepka and Š. Kment, *ACS Appl. Energy Mater.*, 2021, **4**, 6445.
6 J. Luo, X. Wang, S. Li, J. Liu, Y. Guo, G. Niu, L. Yao, Y. Fu, L. Gao, Q. Dong, C. Zhao, M. Leng, F. Ma, W. Liang, L. Wang, S. Jin, J. Han, L. Zhang, J. Etheridge, J. Wang, Y. Yan, E. H. Sargent and J. Tang, *Nature*, 2018, **563**, 541.
7 D. Manna, T. K. Das and A. Yella, *Chem. Mater.*, 2019, **31**, 10063.
8 D. Manna, J. Kangsabanik, T. K. Das, D. Das, A. Alam and A. Yella, *J. Phys. Chem. Lett.*, 2020, **11**, 2113.
9 A. C. Dakshinamurthy and C. Sudakar, *J. Phys. Chem. Lett.*, 2022, **13**, 433.
10 Y. Liu, Y. Jing, J. Zhao, Q. Liu and Z. Xia, *Chem. Mater.*, 2019, **31**, 3333.
11 R. S. Lamba, P. Basera, S. Bhattacharya and S. Sapra, *J. Phys. Chem. Lett.*, 2019, **10**, 5173.
12 Q. Hu, G. Niu, Z. Zheng, S. Li, Y. Zhang, H. Song, T. Zhai and J. Tang, *Small*, 2019, **15**, 1903496.
13 S. Li, H. Wang, P. Yang, L. Wang, X. Cheng and K. Yang, *J. Alloys Compd.*, 2021, **854**, 1.
14 H. Siddique, Z. Xu, X. Li, S. Saeed, W. Liang, X. Wang, C. Gao, R. Dai, Z. Wang and Z. Zhang, *J. Phys. Chem. Lett.*, 2020, **11**, 9572.
15 P. Han, X. Mao, S. Yang, F. Zhang, B. Yang, D. Wei, W. Deng and K. Han, *Angew. Chem., Int. Ed.*, 2019, **58**, 17231.
16 P. Vashishtha, B. E. Griffith, Y. Fang, A. Jaiswal, G. V. Nutan, A. P. Bartók, T. White and J. V. Hanna, *J. Mater. Chem. A*, 2022, **10**, 3562.
17 K. Dave, W. T. Huang, T. Leśniewski, A. Lazarowska, D. Jankowski, S. Mahlik and R. S. Liu, *Dalton Trans.*, 2022, **51**, 2026.
18 Z. Li, F. Sun, H. Song, H. Zhou, Y. zhou, Z. Yuan, P. Guo, G. Zhou, Q. Zhuang and X. Yu, *Dalton Trans.*, 2021, **50**, 9804.
19 F. Locardi, E. Sartori, J. Buha, J. Zito, M. Prato, V. Pinchetti, M. L. Zaffalon, M. Ferretti, S. Brovelli, I. Infante, L. De Trizio and L. Manna, *ACS Energy Lett.*, 2019, **4**, 1976.
20 D. Zhu, J. Zito, V. Pinchetti, Z. Dang, A. Olivati, L. Pasquale, A. Tang, M. L. Zaffalon, F. Meinardi, I. Infante, L. De Trizio, L. Manna and S. Brovelli, *ACS Energy Lett.*, 2020, **5**, 1840.
21 E. T. McClure, M. R. Ball, W. Windl and P. M. Woodward, *Chem. Mater.*, 2016, **28**, 1348.
22 Y. Jia, X. Hou, Z. Wang and X. Hu, *ACS Sustainable Chem. Eng.*, 2021, **9**, 6130.
23 A. Mahmood and J. L. Wang, *Energy Environ. Sci.*, 2021, **14**, 90.
24 K. Min and E. Cho, *J. Phys. Chem. C*, 2020, **124**, 14759.
25 S. Chen, Y. Hou, H. Chen, X. Tang, S. Langner, N. Li, T. Stubhan, I. Levchuk, E. Gu, A. Osvet and C. J. Brabec, *Adv. Energy Mater.*, 2018, **8**, 1.
26 Y. Zhao, J. Zhang, Z. Xu, S. Sun, S. Langner, N. T. P. Hartono, T. Heumueller, Y. Hou, J. Elia, N. Li, G. J. Matt, X. Du, W. Meng, A. Osvet, K. Zhang, T. Stubhan, Y. Feng, J. Hauch, E. H. Sargent, T. Buonassisi and C. J. Brabec, *Nat. Commun.*, 2021, **12**, 1.
27 E. Gu, X. Tang, S. Langner, P. Duchstein, Y. Zhao, I. Levchuk, V. Kalancha, T. Stubhan, J. Hauch, H. J. Egelhaaf, D. Zahn, A. Osvet and C. J. Brabec, *Joule*, 2020, **4**, 1806.
28 F. Akhundova, L. Lüer, A. Osvet, J. Hauch, I. M. Peters, K. Forberich, N. Li and C. Brabec, *Appl. Phys. Lett.*, 2021, **118**, 1ENG.
29 S. Chen, L. Zhang, Y. Liu, Z. Zhang, Y. Li, W. Cai, H. Lv, Y. Qin, Q. Liao, B. Zhou, T. Yan, J. Ren, S. Chen, X. Xiang, S. Dai, S. K. So, X. Wang, S. Yang and B. Xu, *J. Mater. Chem. A*, 2021, **9**, 25502.
30 K. Higgins, M. Ziatdinov, S. V. Kalinin and M. Ahmadi, *J. Am. Chem. Soc.*, 2021, **143**, 19945.
31 M. Ahmadi, M. Ziatdinov, Y. Zhou, E. A. Lass and S. V. Kalinin, *Joule*, 2021, **5**, 2797.
32 A. V. Naumkin, A. Kraut-Vass, S. W. Gaarenstroom and C. J. Powell, *NIST X-ray Photoelectron Spectroscopy Database, NIST*, 2012.
33 Z. Xu, X. Jiang, H. P. Cai, K. Chen, X. Yao and Y. Feng, *J. Phys. Chem. Lett.*, 2021, **12**, 10472.
34 C. Y. Wang, P. Liang, R. J. Xie, Y. Yao, P. Liu, Y. Yang, J. Hu, L. Shao, X. W. Sun, F. Kang and G. Wei, *Chem. Mater.*, 2020, **32**, 7814.

35 C. Würth, C. Lochmann, M. Spieles, J. Pauli, K. Hoffmann, T. Schüttrigkeit, T. Franzl and U. Resch-Genger, *Appl. Spectrosc.*, 2010, **64**, 733.
36 L. De Trizio, I. Infante, A. L. Abdelhady, S. Brovelli and L. Manna, *Trends Chem.*, 2021, **3**, 631.
37 J. Klafter and M. F. Shlesinger, *Proc. Natl. Acad. Sci. U. S. A.*, 1986, **83**, 848.
38 R. Chen, *J. Lumin.*, 2003, **102–103**, 510.
39 J. E. Thomaz, K. P. Lindquist, H. I. Karunadasa and M. D. Fayer, *J. Am. Chem. Soc.*, 2020, **142**, 16622.

